Published in "Physical Review B 94(5): 054423, 2016
which should be cited to refer to this work.

Coexisting multiple order parameters in single-layer $LuMnO_3$ films

Christof W. Schneider,[1,*] Saumya Mukherjee,[2] Kenta Shimamoto,[1] Saikat Das,[3] Hubertus Luetkens,[4] Jonathan S. White,[2] Matthias Bator,[1] Yi Hu,[1] Jochen Stahn,[2] Thomas Prokscha,[4] Andreas Suter,[4] Zaher Salman,[4] Michel Kenzelmann,[5] Thomas Lippert,[1,6] and Christof Niedermayer[2,†]

[1]*Energy and Environment Research Department, Paul Scherrer Institut, CH-5232 Villigen PSI, Switzerland*
[2]*Laboratory for Neutron Scattering and Imaging, Paul Scherrer Institut, CH-5232 Villigen PSI, Switzerland*
[3]*University of Fribourg, Department of Physics and Fribourg Centre for Nanomaterials, Chemin du Musée 3, CH-1700 Fribourg, Switzerland*
[4]*Laboratory for Muon Spin Spectroscopy, Paul Scherrer Institut, CH-5232 Villigen PSI, Switzerland*
[5]*Laboratory for Scientific Developments and Novel Materials, Paul Scherrer Institut, CH-5232 Villigen PSI, Switzerland*
[6]*Department of Chemistry and Applied Biosciences, Laboratory of Inorganic Chemistry, ETH Zurich, CH 8093 Zurich, Switzerland*

Magnetoelectric multiferroics hold great promise for electrical control of magnetism or magnetic control of ferroelectricity. However, single phase ferroelectric materials with a sizeable ferromagnetic magnetization are rare. Here, we demonstrate that a single-phase orthorhombic $LuMnO_3$ thin film features coexisting magnetic and ferroelectric orders. The temperature dependence of the different order parameters are presented with ferromagnetic order appearing below 100 K and thus at much higher temperatures than ferroelectricity or antiferromagnetism ($T_N, T_{FE} \leqslant 40$ K).

I. INTRODUCTION

Ferromagnetic (FM) ferroelectrics (FEs) are of potential interest for device applications such as information storage, spintronics, microwave tunable devices, or sensors because of their fast dynamics and energy efficient multifunctional properties [1]. These materials are called multiferroics and feature, e.g., coupled magnetic and FE orders that can open a way to switch a magnetic moment, μ, by an electric field and vice versa [2,3]. Experimentally, only very few multiferroic materials are known to be FM [1,4–6] with the large majority being antiferromagnetically ordered. Multiferroic materials can be roughly classified into two groups depending on whether the origin of magnetic and FE order is independent or not. Materials that belong to the first category, e.g., $BiFeO_3$, offer high transition temperatures while the magnetoelectric coupling is weak. The other group has the same origin for magnetic and FE order, which results in a strong magnetoelectric coupling often combined with low transition temperatures. To achieve a more efficient and direct switching of the magnetization by an applied electric field, preparing FM multiferroics, which belong to the latter group, is desirable [7].

Future applications of multiferroic materials will heavily rely on thin films, as is the case for other advanced materials used in applications [8–14]. Switching the magnetization with an applied electric field using multiferroic materials is attempted by preparing heterostructures of, e.g., multiferroic and FM thin films, as shown for $CoFe/BiFeO_3$ bilayers [15]. So far, artificially layered structures are likely to suffer from fatigue, a time dependent aging effect. One potential solution for this problem is to find FM-multiferroic materials that can be grown heteroepitaxially as thin film. The lattice mismatch between the film and the substrate gives various options to generate FM, such as a strained lattice and creating dislocations [16–21].

We have previously shown that orthorhombic $LuMnO_3$ (o-LMO, *Pbnm* space group) films epitaxially grown on $YAlO_3$ (110) substrates have two coexisting and exchange biased magnetic ground states in a single thin film (ferro- and antiferromagnetism) [22]. As a bulk material, o-LMO exhibits spin-driven FE with an E-type ($q_k = 0.5$) spin structure below 35 K, and the electrical polarization, P, is pointing along the crystallographic [100] direction [23]. In our o-LMO films, a FM interface layer $\approx$10 nm thick has been measured with a magnetic moment of $\approx 1\mu_B$/Mn, decaying toward the film surface with a total moment of $\approx\langle 0.5\rangle\mu_B$/Mn in addition to incommensurate (IC) antiferromagnetic (AFM) ordering [22,24]. Due to reported values of q_k close to 0.5 for $LuMnO_3$ films, it is speculated that there is a coexistence of a cycloidal and an E-type state [24], as is suspected for (010) $YMnO_3$ films [17].

Here, we investigate and discuss the different order parameters (FM, AFM, FE) in (110) o-LMO and their respective temperature dependencies. A wide range of measurement techniques is necessary to capture all aspects of the intricate and coupled nature of the different orders. By measuring the temperature dependence of the local magnetic field of ordered Mn moments in zero field (ZF) using low energy muon spin relaxation (LE-μSR), we are able to outline a magnetic phase diagram. Neutron diffraction is sensitive to AFM by measuring the magnetic ordering vector q_k, whereas temperature dependent magnetic susceptibility measurements provide integral information about the presence of antiferromagnetism and ferromagnetism in the film. Finally, FE properties are investigated using a direct measurement of P, which is the result of breaking the inversion symmetry of the crystalline structure.

II. EXPERIMENT

Epitaxial thin films of single-phase o-LMO were grown on (110)-oriented $YAlO_3$ [22] single crystalline substrates by pulsed laser deposition using a KrF excimer laser. Details

*Corresponding author: christof.schneider@psi.ch
†Corresponding author: christof.niedermayer@psi.ch
The authors declare that they have no competing financial interests.

of the deposition process can be found elsewhere [22,25]. The film thicknesses investigated were ≈200 nm for $P(T)$ measurement, 400 nm o-LMO for neutron diffraction, and 56 nm for LE-μSR.

Muon spin rotation/relaxation experiments were conducted at the μE4 low energy muon beam line at the Paul Scherrer Institut. This beamline produces spin polarized muons with a tuneable energy between 1 and 30 keV [26–29]. For the experiments described in this paper, muons with an energy of 4.1 keV were implanted near the center of a 56 nm (110) o-LMO film. Muons act as very sensitive local probes of internal magnetic fields, which can be monitored via the time evolution of the muon spin polarization [30]. The μSR data were analyzed with the free software package MUSRFIT [31].

Neutron diffraction experiments were performed on the triple-axis spectrometer RITA-II at the Swiss spallation neutron source SINQ, Paul Scherrer Institut, Villigen, Switzerland. A 400-nm-thick (110) LMO film was mounted in the (0k0-00l) scattering plane, which provides access to the strongest magnetic peaks, e.g., (0 ½ 1) for an E-type AFM structure [32]. The measurements at RITA-II were performed at a neutron wavelength $\lambda = 4.21$ Å. A pyrolytic graphite filter between monochromator and sample together with a Be filter between sample and analyzer were installed to suppress higher order contamination.

Magnetization curves were obtained with a commercial Quantum Design Physical Property Measurements System (QD-PPMS-9) vibrating sample magnetometer. The samples were cooled down to 10 K in ZF before starting the measurements. Coercive fields were derived by sweeping the magnetic field up to 4 T for each temperature.

The temperature dependent remnant polarization for (110) o-LMO thin films was measured using a Sawyer-Tower circuit and the Positive-Up Negative-Down method, as described in Ref. [33]. Interdigitated electrodes were prepared by optical lithography and a lift-off process having 351 fingers, each 1.25 mm long and 5 μm wide with 5 μm spacing. This structure is sensitive to the [1$\bar{1}$0] and [001] in-plane directions of the film when pattering two identical structures, turned by 90°, onto the film surface along the crystallographic axes. The samples are measured in a helium exchange gas environment by accurately controlling the measurement temperature (Lakeshore temperature controller model 325) with the fastest temperature ramp being 1 K min^{-1}. For each data point the temperature was kept stable within 0.1 K.

III. RESULTS

A. Magnetic characterization

Using LE-μSR to probe the temperature dependent magnetic properties of (110) LMO films, the outline of a magnetic phase diagram can be traced. In Fig. 1(a), we show the time evolution of the muon spin polarization measured in zero external field for various temperatures. Whereas the time evolution of the muon spin polarization at 100 K and 75 K is very similar and characterized by small relaxation rates, the relaxation rates at 60 K and 45 K, respectively, are considerably larger, indicating the formation of a strong local magnetic field in the film associated with significant magnetic

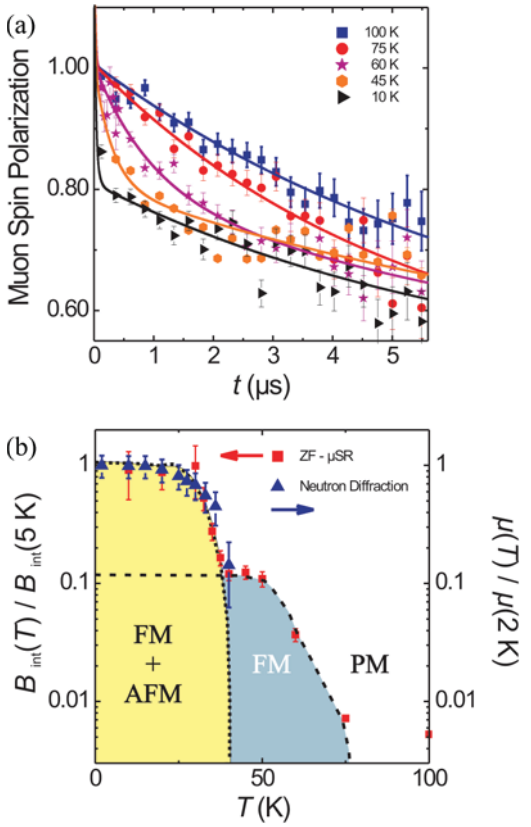

FIG. 1. (a) Muon spin polarization vs time in zero field at 100, 75, 60, 45, and 10 K. The solid lines are fits to the measured data. (b) Temperature dependence of the normalized internal magnetic field $B_{\rm int}(T)/B_{\rm int}(5K)$ as derived from ZF-μSR muon spin relaxation measurements with low energy muons implanted with 4.1 keV into a 56-nm-thin (110) $LuMnO_3$ thin film. For comparison, the normalized magnetic moment $\mu(T)/\mu(2\,\mathrm{K})$ vs T is shown (blue triangle), with μ being proportional to the square root of the integrated neutron intensity. The black dashed lines for the FM and AFM phase are a guide to the eye but also indicate how the temperature dependence of a single order parameter could look like when both orders coexist.

moments. A very rapid decay of the muon spin polarization is observed at 10 K, signaling the presence of a very broad distribution of internal magnetic fields. At low temperatures, the spectra show a progressively stronger two component relaxation (damping), which is typical for the development of (quasi) static magnetic order [30].

Due to the smallness of the sample compared to the low energy muon (LEM) beam spot, the spectra contain a 50% fraction of muons stopping in the Ag sample holder. This fraction of the signal is not changing with temperature and is practically nonrelaxing. The remaining $LuMnO_3$ signal is described by the two component fit function $P(t) = f_{\rm fast}e^{-\lambda_{\rm fast}t} + (1 - f_{\rm fast})\,e^{-\lambda_{\rm slow}t}$ [30]. At high temperatures, the spectra follow a single exponential relaxation function indicating that the system is in a fast fluctuating magnetic state. Only below 75 K does part of the signal show a very fast damping with a relaxation rate $\lambda_{\rm fast}$, whereas the second component remains slowly relaxing with a rate $\lambda_{\rm slow}$. The fast fraction $f_{\rm fast} = 0.37$ is obtained from a global data fitting routine where all measured temperatures were fitted

simultaneously while the two exponential relaxation rates are determined for each temperature. In a long range ordered magnet, the muon spin polarization is often found to oscillate due to the muon spin precession in the local magnetic field $B_{\rm int}$. In a nonuniform magnetic situation like in the present case, only an overdamped oscillation or simply an exponential relaxation is observed. In this situation, $\lambda_{\rm fast}$ corresponds to the so-called transverse relaxation rate of muons stopping in a strongly magnetic environment of the film.

The transverse relaxation rate is associated with the distribution of internal magnetic fields. It is possible to estimate the typical size of the internal fields, which are of the order of $B_{\rm int} \approx \lambda_{\rm fast}/\gamma$ with the muon's gyromagnetic ratio $\gamma/2\pi = 135.4\,{\rm MHz\,T^{-1}}$. Converting the relaxation rates for all temperatures measured into $B_{\rm int}$, the $B_{\rm int}(T)/B_{\rm int}(5K)$ diagram shows two distinct successive magnetic transitions [Fig. 1(b)]. There is a clear rise of $B_{\rm int}$ between 75 and 50 K reaching a small plateau down to 40 K before rising a second time with a saturation of $B_{\rm int}$ starting at 30 K. The transition starting between 75 and 100 K is associated with the appearance of FM order [22], and the plateau starting at ≈50 K would correspond to a saturation of the magnetic moment. The second transition observed ≈40 K agrees well with the onset of antiferromagnetism in LMO films and bulk [22–24,34]. It is important to note that a zero magnetic field μSR measurement provides a true microscopic confirmation of a magnetic ground state, i.e., the magnetic component is not induced by the application of an external magnetic field. We can therefore consider that the contours of the $B_{\rm int}(T)/B_{\rm int}(5K)$ vs T measurement reflect phase boundaries of a FM and an AFM phase in (110) o-LMO films. While our local probe approach clearly defines the onset of (quasi) static magnetism, the exact nature of the FM ground state cannot be determined with respect to the length scale of the FM correlations.

The interpretation of $\lambda_{\rm slow}$ is not straightforward for an intrinsically inhomogeneous sample. It can contain contributions from muons stopping in weakly magnetic regions of the sample and/or dynamic effects. In principle, the two scenarios can be distinguished by longitudinal field experiments [30]. The limited size of the sample together with the geometrical constraints of the LEM detector setup did not allow us to draw definitive conclusions.

The AFM ordering was studied by neutron diffraction. Figure 2(a) shows elastic q scans of the AFM (0 q_k 1) Bragg peak along the [0k0] direction of a 400 nm (110) o-LMO film between 2 and 45 K. In Fig. 2(b), we plot the integrated intensity vs T and q vs T as derived from Gaussian fits to the data. The temperature dependence of the AFM order parameter represented as integrated intensity vs T defines a magnetic transition at $T_{\rm N} \approx 40\,{\rm K}$. The integrated intensity is proportional to μ^2 and rises with decreasing temperature before saturating below 15 K. Comparing the temperature dependence of the AFM order parameter as $\mu(T)/\mu(2\,{\rm K})$ with the μSR measurement in Fig. 1(b) shows good agreement, thereby confirming the AFM phase measured using ZF-μSR. Similar to the $q_{\rm k}$ measurements reported in Ref. [22], the width of the AFM peak is not resolution limited with a resolution-corrected magnetic correlation length of ≈15 nm along the crystallographic b direction. This magnetic correlation length

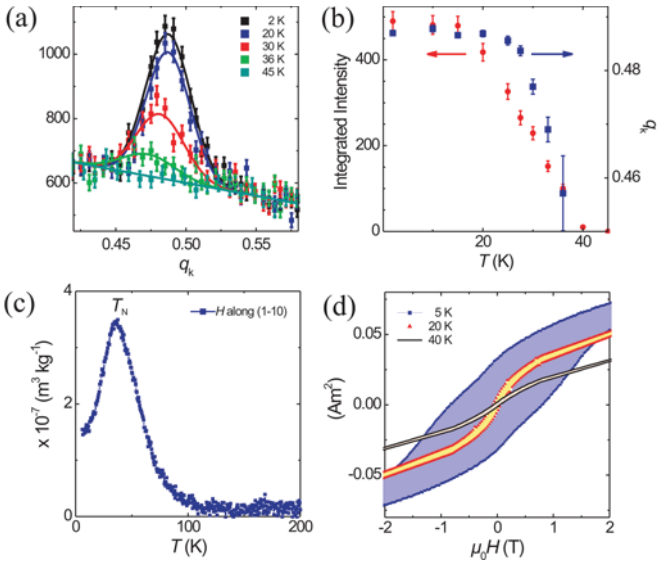

FIG. 2. (a) q-scans for the AFM (0 ≈ 0.5 1) Bragg peak of a 400 nm (110) LMO film with an area of 8 × 10 mm measured at different temperatures. (b) Integrated neutron intensity vs temperature for the AFM (0 ≈ $q_{\rm k}$1), $q_{\rm k} \approx 0.5$ (r.l.u.) (red dots). The magnetic ordering wave vector is $q_{\rm k} = 0.488$ at 1.6 K and $T_{\rm N} \approx 40\,{\rm K}$. The temperature dependence of $q_{\rm k}$ is extracted from the same data set (blue square). (c) Susceptibility vs temperature for a 56-nm-thin (110) $LuMnO_3$ thin film with $H = 30\,{\rm mT}$ along [1$\bar{1}$0]. The AFM transition temperature $T_{\rm N}$ is ≈36 K. (d) $M(H)$ loops measured at 5, 20, and 40 K for a 56-nm-thin (110) $LuMnO_3$ thin film with H along [1$\bar{1}$0].

corresponds roughly to the size of the AFM domains in these films. We also note that there is no sign of a second magnetic transition below $T_{\rm N}$, in contrast to the behavior observed in bulk [35], indicating that the magnetic phases of o-LMO thin films behave differently as compared to bulk. In Fig. 2(b), we also show the temperature dependence of $q_{\rm k}$ extracted from the same data set. There is a steep increase of $q_{\rm k}$ with decreasing temperature up to 28 K before the value of $q_{\rm k}$ saturates at lower temperatures with $q_{\rm k} = 0.488$ (r.l.u.) at 2 K [Fig. 2(a)]. This is in clear contrast to AFM properties as compared to bulk o-LMO, which exhibits commensurate E-type ordering ($q_{\rm k} = 0.5$) below 35 K [35,36].

The ZF-cooled (ZFC) susceptibility was measured along the [1$\bar{1}$0] in-plane direction for a 56 nm (110) o-LMO film showing an AFM transition at ≈36 K [Fig. 2(c)]. The susceptibility is starting to rise well above $T_{\rm N}$, indicating a potential FM contribution. To define the onset of this magnetic transition and to verify ferromagnetism above $T_{\rm N}$, magnetic hysteresis loops have been measured at several temperatures [Fig. 2(d)]. The saturation magnetization decreases with increasing temperature and vanishes around $T \approx 80\,{\rm K}$, which also agrees by interpolating the steepest slope of the susceptibility data from Fig. 2(c) to intercept with the temperature axis. Measuring the $YAlO_3$ substrate alone under the same experimental conditions proves that the small hysteresis measured below 90 K is intrinsic to the o-LMO film and not produced by a remnant field of the apparatus or magnetic impurities. This temperature is identified as $T_{\rm C}$, the FM ordering temperature, and is consistent with ZF-μSR

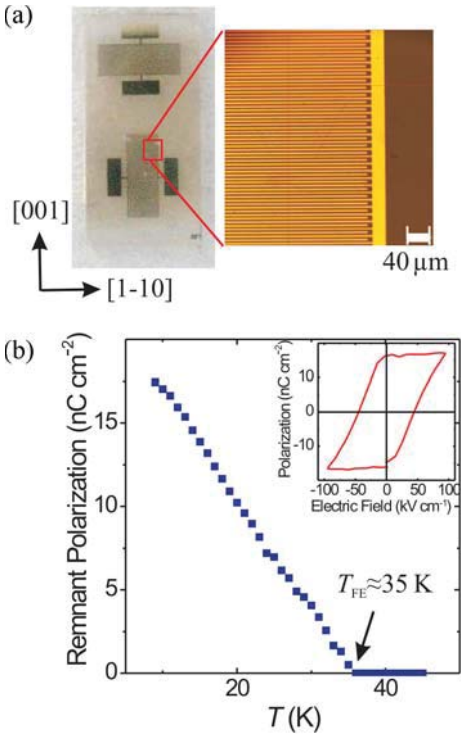

FIG. 3. (a) Optical photograph of interdigitated electrodes patterned on a (110) oriented $LuMnO_3$ thin film. The two patterns are aligned along the main *in-plane* crystallographic axis of the substrate. (b) Remnant electric polarization for a 200 nm (110) $LuMnO_3$ film. P was measured along the $[1\bar{1}0]$ in-plane direction with $T_{FE} \approx 35$ K. In the inset, a $P(E)$ loop measured along $[1\bar{1}0]$ at 10 K is shown.

measurements on the same film shown in Fig. 1. These magnetization measurements therefore establish an onset of the FM order at relatively high temperatures independent of the AFM order observed below $T \approx 40$ K [22,24]. In addition, the magnetization measurements show that the ferromagnetism in our films is relatively soft above $T \approx 40$ K but becomes harder with decreasing temperatures.

B. FE characterization

The temperature dependent remnant polarization, $P(T)$, was measured using an interdigitated structure, which was patterned onto the film surface along the in-plane crystallographic axes of the substrate [see Fig. 3(a)]. Figure 4(b) shows $P(T)$ measured along the $[1\bar{1}0]$ in-plane direction in a 200-nm-thick (110) *o*-LMO film with an onset at ≈35 K. This onset defines the FE transition temperature T_{FE} for our *o*-LMO films, which is similar, as reported for bulk [23]. Below T_{FE}, clearly identifiable $P(E)$ loops are observed, as shown in the inset of Fig. 3(b). These measurements are the first direct proof of FE in epitaxial *o*-LMO films, vindicating the interpretation that the experimentally observed crystalline distortion using hard x rays in *o*-LMO thin films below T_N is leading indeed to a spontaneous FE polarization [24].

C. Discussion

We briefly summarize the different orders in (110) *o*-LMO thin films, including the results from Refs. [22] and [24]: Single crystallinelike (110) *o*-LMO films show two independent

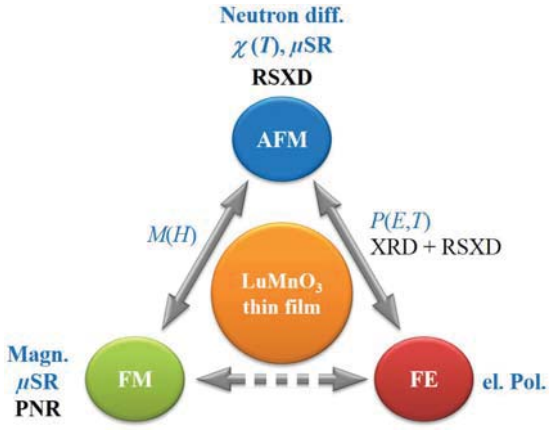

FIG. 4. Sketch of a ferroic triangle showing the relation and techniques with which the ferroic orders, FM, AFM, and FE, and their mutual coupling have been established. The experimental techniques written in black letters (polarized neutron reflectometry, PNR; resonant soft x-ray diffraction, SXRD; x-ray diffraction, XRD) to identify ferroic properties have been reported elsewhere [22,24]. Magnetization, susceptibility, μSR, neutron diffraction, and electrical polarization are reported in the text.

magnetic ground states with FM setting in at ≈80 K and AFM at ≈40 K. In addition, these films are FE with $T_{FE} \approx 35$ K. The AFM ground state is IC with a q_k value for the magnetic ordering vector smaller than expected for E-type ordering ($q_k = 0.5$). Further, ferromagnetism is located within a thin layer at the film – substrate interface [22]. The FM layer is exchange-coupled to antiferromagnetism [22], and there is a correlation between the c axis component of the AFM ordered Mn spins and structural distortion due to the symmetry breaking [24].

With respect to ferroelectricity in (110) *o*-LMO thin films, we note two differences of the FE properties compared to what has been observed for bulk specimens. First, the remnant polarization along $[1\bar{1}0]$ is at most 20 nC cm^{-2} and clearly much smaller than expected for bulk E-type orthorhombic $RE\mathrm{MnO_3}$(≈460 nC cm^{-2}) [23], Even if we assume that what we observed was a projection of a potential a axis polarization, the measured value is still very small. Potential origins of the strongly reduced polarization are either related to strain and defects in the film or the main contribution of the FE polarization is different from bulk like an inverse Dzyaloshinskii-Moriya interaction because of the IC AFM ordering [37]. The origin of the large polarization for an E-type o-$RE\mathrm{MnO_3}$ is theoretically explained and experimentally shown to be a consequence of shifted atoms due to the symmetric magnetostriction, which accompanies the stabilization of the E-type magnetic order [38,39]. Strain and defects may disturb the movement of atoms significantly, and changes to the electronic contribution to the FE polarization may be observed as a consequence. Most o-$RE\mathrm{MnO_3}$ films (RE = Tb, Ho, Lu, Tm) investigated with a (110) as well as (010) orientation show a q_k close to 0.5 [22,24,40,41], the commensurate value for an E-type, and (010) oriented films have an electrical polarization compatible with an E-type. This contradiction of large values of P, requiring a symmetric exchange interaction, and an overall IC magnetic ordering

albeit being close to commensurate suggesting an asymmetric interaction, is difficult to explain. We therefore propose the scenario of a coexisting symmetric magnetostriction mechanism and an inverse Dzyaloshinskii-Moryia interaction in our films. If the fragmentation of different interaction regions is organized in a layered fashion or in terms of domains needs to be clarified. To explain the small polarization values for (110) $LuMnO_3$, an inverse Dzyaloshinskii-Moriya interaction cannot be ruled out fully. However, crystalline quality, strain, and defects [41], as well as composition [42], are considered to be more likely to influence the value of P in these nominal E-type antiferromagnets rather than a dominant asymmetric exchange interaction if q_k is close to commensurate.

Second, the almost linear increase of $P(T)$ is highly unusual and not compatible with measurements on bulk samples [23,43]. This temperature dependence is reminiscence to an incipient FE behavior as it was observed for strained $CaMnO_3$ thin films using an optical approach to probe the polar state [44]. Further, the size of FE domains will be determined by the size of the AFM domains, which are of the order 15 nm as a consequence of the short magnetic correlation length. This length scale seems to be determined by structural defect [22], which may also have an effect on the magnitude and possibly on the temperature dependence of P. However, the origin of $P(T)$ for (110) o-LMO is still under investigation.

The potential origin of ferromagnetism in o-LMO and possible consequences of $T_C > T_N$ in a single phase material with an AFM ground state are discussed next. So far, there are three different scenarios that can lead the ferromagnetism in these materials: spin canting, spin frustration, or defects. Canting or spin frustration as the cause of FM would result in $T_C \leqslant T_N$ because the observed ferromagnetism is a direct consequence of the AFM ground state. Spin canting along the [001] direction of the LMO unit cell is present, which enables us to measure the magnetic diffraction peak at (0 q_k 0) using resonant soft x-ray diffraction, but FM is not reported [17,24]. A FM interlayer coupling [45] between antiferromagnetically arranged layers or defects therein [20,46] is also conceivable and would equally result in $T_C \leqslant T_N$. Both scenarios are in contrast to the observed order of the respective transition temperatures. Another potential origin for FM are changes in the Mn-O-Mn bonding angles leading to a deformation of, e.g., the oxygen octahedra at a perovskite heterointerface, as reported for the $SrRuO_3/GdScO_3$ system [47]. The rearranged oxygen octahedra of o-LMO connecting to the YAO substrate could modify the exchange interactions as well as the orbital occupation between Mn spins and hence form a FM layer at the film-substrate interface with $T_C > T_N$. So far, calculations did not show any indication that a change in bonding angle gives rise to ferromagnetism, a mechanism which would have been at present the most likely scenario for ferromagnetism with $T_C > T_N$ in combination with growth induced strain [48].

IV. CONCLUSIONS

We studied the coexisting FE, FM, and AFM properties and orders for (110) oriented o-$LuMnO_3$ thin films, which can also be cross-coupled with $T_C > T_N > T_{FE}$. The ferroic triangle (Fig. 4) illustrates the relation of the three order parameters and how the different orders' mutual coupling is identified. The temperature dependences of the FM and AFM orders have been traced using ZF-μSR measurements. The FM ordering takes place with $T_C \approx 80$ K, followed by AFM ordering at $\approx$40 K. The measured temperature dependence of the AFM order parameter using neutron scattering agrees well with the μSR measurements, thus confirming the aforementioned nature of the transition below 40 K in ZF-μSR measurements. In addition, polar ordering has been established for $T_{FE} \approx 35$ K, as evidenced by $P(T)$ measurements. Showing AFM order using neutron diffraction and polar order as a result of a structural symmetry breaking [24], confirms that magnetism drives ferroelectricity and hence shows the coupled nature of these two orders. Likewise, FM–AFM coupling was established by measuring the exchange bias [22].

So far, all investigated (110) o-LMO films show IC AFM ordering. The IC value of the magnetic ordering vector is attributed to a combination of tensile and compressive strain as well as defects in these films. These defects are also suspected to be the origin of a significant reduction of the electrical polarization as compared to bulk values, and the strained lattice may limit the movement of the oxygen and manganese atoms in the ab plane when the structural phase transition takes place, leading to ferroelectricity. Future studies will address the question toward the origin of the prominent FM phase, which is largely confined to a thin layer next to the film-substrate interface [22] and whether this FM phase has long-range order. Also, the missing link in the triangle, a possible FE–FM coupling will be investigated in detail. To resolve the issue of a potentially mixed cycloidal/E-type state, an analysis of the magnetic structure for such films is required.

ACKNOWLEDGMENTS

This paper is based on experiments performed at the Swiss Spallation Neutron Source (SINQ) and the Swiss Muon Source (SμS), Paul Scherrer Institute (PSI), Villigen, Switzerland. Support of this paper by the PSI through the Forschungskommission and Schweizerischer Nationalfonds zur Förderung der Wissenschaftlichen Forschung (No. 200021_147049), in particular the National Center of Competence in Research, Materials with Novel Electronic Properties (MaNEP) is gratefully acknowledged. We thank Ch. Bernhard, M. Fiebig, M. Trassin, N. Spaldin, and N. Fedorova for their valuable input and discussions.

[1] J. H. Lee, L. Fang, E. Vlahos, X. Ke, Y. W. Jung, L. F. Kourkoutis, J.-W. Kim, P. J. Ryan, T. Heeg, M. Roeckerath, V. Goian, M. Bernhagen, R. Uecker, P. C. Hammel, K. M. Rabe, S. Kamba, J. Schubert, J. W. Freeland, D. A. Muller, C. J. Fennie *et al.*, Nature **466**, 954 (2010).

[2] D. Khomskii, Physics **2**, 20 (2009).

[3] N. A. Spaldin and M. Fiebig, Science **309**, 391 (2005).
[4] W. Eerenstein, N. D. Mathur, and J. F. Scott, Nature **442**, 759 (2006).
[5] R. Ramesh and N. A. Spaldin, Nat. Mater. **6**, 21 (2007).
[6] Y. Tokunaga, Y. Taguchi, T.-h. Arima, and Y. Tokura, Nat Phys **8**, 838 (2012).
[7] N. A. Hill, J. Phys. Chem. B **104**, 6694 (2000).
[8] J.-M. Hu, L.-Q. Chen, and C.-W. Nan, Advanced Materials **28** 15 (2016).
[9] J. Fortin and A. Zribi, *Functional Thin Films and Nanostructures for Sensors* (Springer, United States, 2009).
[10] B. Xu, D. Wang, H. J. Zhao, J. Íñiguez, X. M. Chen, and L. Bellaiche, Adv. Funct. Mater. **25**, 3626 (2015).
[11] D. H. Kim, X. Y. Sun, N. M. Aimon, J. J. Kim, M. J. Campion, H. L. Tuller, L. Kornblum, F. J. Walker, C. H. Ahn, and C. A. Ross, Adv. Funct. Mater. **25**, 3091 (2015).
[12] D. H. Kim, N. M. Aimon, X. Y. Sun, L. Kornblum, F. J. Walker, C. H. Ahn, and C. A. Ross, Adv. Funct. Mater. **24**, 5889 (2014).
[13] J. Ma, J. Hu, Z. Li, and C.-W. Nan, Adv. Mater. **23**, 1062 (2011).
[14] J. F. Scott, J. Mater. Chem. **22**, 4567 (2012).
[15] Z. Zhou, M. Trassin, Y. Gao, Y. Gao, D. Qiu, K. Ashraf, T. Nan, X. Yang, S. R. Bowden, D. T. Pierce, M. D. Stiles, J. Unguris, M. Liu, B. M. Howe, G. J. Brown, S. Salahuddin, R. Ramesh, and N. X. Sun, Nat. Commun. **6**, 6082 (2015).
[16] D. Rubi, C. de Graaf, C. J. M. Daumont, D. Mannix, R. Broer, and B. Noheda, Phys. Rev. B **79**, 014416 (2009).
[17] H. Wadati, J. Okamoto, M. Garganourakis, V. Scagnoli, U. Staub, Y. Yamasaki, H. Nakao, Y. Murakami, M. Mochizuki, M. Nakamura, M. Kawasaki, and Y. Tokura, Phys. Rev. Lett. **108**, 047203 (2012).
[18] I. Fina, L. Fabrega, X. Marti, F. Sanchez, and J. Fontcuberta, Appl. Phys. Lett. **97**, 232905 (2010).
[19] C. J. M. Daumont, D. Mannix, V. Sriram, G. Catalan, D. Rubi, B. J. Kooi, J. T. M. D. Hosson, and B. Noheda, J. Phys.: Condens. Matter **21**, 182001 (2009).
[20] S. Farokhipoor, C. Magen, S. Venkatesan, J. Iniguez, C. J. M. Daumont, D. Rubi, E. Snoeck, M. Mostovoy, C. de Graaf, A. Muller, M. Doblinger, C. Scheu, and B. Noheda, Nature **515**, 379 (2014).
[21] X. Marti, V. Skumryev, V. Laukhin, R. Bachelet, C. Ferrater, M. V. Garcia-Cuenca, M. Varela, F. Sanchez, and J. Fontcuberta, J. Appl. Phys. **108**, 123917 (2010).
[22] J. S. White, M. Bator, Y. Hu, H. Luetkens, J. Stahn, S. Capelli, S. Das, M. Dobeli, T. Lippert, V. K. Malik, J. Martynczuk, A. Wokaun, M. Kenzelmann, C. Niedermayer, and C. W. Schneider, Phys. Rev. Lett. **111**, 037201 (2013).
[23] S. Ishiwata, Y. Kaneko, Y. Tokunaga, Y. Taguchi, T.-h. Arima, and Y. Tokura, Phys. Rev. B **81**, 100411 (2010).
[24] Y. W. Windsor, S. W. Huang, Y. Hu, L. Rettig, A. Alberca, K. Shimamoto, V. Scagnoli, T. Lippert, C. W. Schneider, and U. Staub, Phys. Rev. Lett. **113**, 167202 (2014).
[25] M. J. Montenegro, K. Conder, M. Döbeli, T. Lippert, P. R. Willmott, and A. Wokaun, Appl. Surf. Sci. **252**, 4642 (2006).
[26] E. Morenzoni, F. Kottmann, D. Maden, B. Matthias, M. Meyberg, T. Prokscha, T. Wutzke, and U. Zimmermann, Phys. Rev. Lett. **72**, 2793 (1994).
[27] P. Bakule and E. Morenzoni, Contemp. Phys. **45**, 203 (2004).
[28] T. Prokscha, E. Morenzoni, K. Deiters, F. Foroughi, D. George, R. Kobler, A. Suter, and V. Vrankovic, Nucl. Instrum. Methods. Phys. Res., Sect. A. **595**, 317 (2008).
[29] https://www.psi.ch/low-energy-muons/lem-low-energy-muons-group.
[30] A. Yaouanc and P. Dalmas de Réotier, *Muon Spin Rotation, Relaxation and Resonance* (Oxford University Press, Oxford, 2010).
[31] A. Suter and B. M. Wojek, Phys. Procedia **30**, 69 (2012).
[32] V. Y. Pomjakushin, M. Kenzelmann, A. Dönni, A. B. Harris, T. Nakajima, S. Mitsuda, M. Tachibana, L. Keller, J. Mesot, H. Kitazawa, and E. Takayama-Muromachi, New J. Phys. **11**, 043019 (2009).
[33] M. Fukunaga and Y. Noda, J. Phys. Soc. Jpn. **77**, 064706 (2008).
[34] H. Okamoto, N. Imamura, B. C. Hauback, M. Karppinen, H. Yamauchi, and H. Fjellvåg, Solid State Commun. **146**, 152 (2008).
[35] M. Garganourakis, Y. Bodenthin, R. A. de Souza, V. Scagnoli, A. Dönni, M. Tachibana, H. Kitazawa, E. Takayama-Muromachi, and U. Staub, Phys. Rev. B **86**, 054425 (2012).
[36] V. Y. Pomjakushin, Personal communication (2015).
[37] T. Kimura, T. Goto, H. Shintani, K. Ishizaka, T. Arima, and Y. Tokura, Nature **426**, 55 (2003).
[38] M. Mochizuki, N. Furukawa, and N. Nagaosa, Phys. Rev. B **84**, 144409 (2011).
[39] D. Okuyama, S. Ishiwata, Y. Takahashi, K. Yamauchi, S. Picozzi, K. Sugimoto, H. Sakai, M. Takata, R. Shimano, Y. Taguchi, T. Arima, and Y. Tokura, Phys. Rev. B **84**, 054440 (2011).
[40] Y. W. Windsor, M. Ramakrishnan, L. Rettig, A. Alberca, E. M. Bothschafter, U. Staub, K. Shimamoto, Y. Hu, T. Lippert, and C. W. Schneider, Phys. Rev. B **91**, 235144 (2015).
[41] K. Shimamoto, Y. W. Windsor, Y. Hu, M. Ramakrishnan, A. Alberca, E. M. Bothschafter, L. Rettig, T. Lippert, U. Staub, and C. W. Schneider, Appl. Phys. Lett. **108**, 112904 (2016).
[42] K. Shimamoto, M. Doebeli, T. Lippert, and C. W. Schneider, J. Appl. Phys. **119**, 184102 (2016).
[43] Y. S. Chai, Y. S. Oh, L. J. Wang, N. Manivannan, S. M. Feng, Y. S. Yang, L. Q. Yan, C. Q. Jin, and K. H. Kim, Phys. Rev. B **85**, 184406 (2012).
[44] T. Günter, E. Bousquet, A. David, P. Boullay, P. Ghosez, W. Prellier, and M. Fiebig, Phys. Rev. B **85**, 214120 (2012).
[45] W. Kuch, L. I. Chelaru, F. Offi, J. Wang, M. Kotsugi, and J. Kirschner, Nat Mater **5**, 128 (2006).
[46] K. Rainey, J. Chess, J. Eixenberger, D. A. Tenne, C. B. Hanna, and A. Punnoose, J. Appl. Phys. **115**, 17D727 (2014).
[47] R. Aso, D. Kan, Y. Shimakawa, and H. Kurata, Sci. Rep. **3**, 2214 (2013).
[48] N. Spaldin, Personal communication (2015).